Non Invasive Thermal Imaging of GaAs MESFET's

Marc Paul de Boer, Hans Winkel, Jasper Verduyn Frank L.M. van den Bogaart, Jan S. de Vries

TNO - Physics and Electronics Laboratory
P.O Box 96864
NL-2509 JG 's-Gravenhage
The Netherlands
Telephone: ++31 70 3264221 ext 210
Telefax: ++31 70 3280961
E-Mail: vandenBogaart@fel.tno.nl
J.S.deVries@fel.tno.nl

ABSTRACT

We demonstrate the use of an infrared focal plane array (IR-FPA) to measure the spatially-resolved surface temperature of a GaAs MESFET (gallium arsenide metal-semiconductor field-effect transistor) under DC and RF operating conditions. By compensating for variations of the small emissivity, absolute temperatures of ± 5 °C, and small temperature differences of 1 °C can be determined. By deconvolution of the lens MTF (modulation transfer function) we attain a resolution of 6.25 μ m. The combination of thermal and spatial sensitivity makes our set-up ideally suited for non-destructive characterisation of semiconductor devices.

1. INTRODUCTION

Spatially resolved temperature measurements are an important tool for the diagnostic testing of many semiconductor devices, since the operation of such devices is often limited by thermal constraints. Such devices should preferably be studied in a non invasive and non destructive manner, i.e. the device operation should neither be affected by the measurement taking place, nor should the device be altered by the measurement. Since infrared imaging fulfils both of these requirements it is a promising candidate for such temperature measurements.

In the past, temperature measurements of semiconductor devices using infrared microscopes or scanning infrared cameras have been reported 1,2,3,4. We believe, however, that the experiment described in this Paper incorporates three major improvements over previous measurements on semiconductor devices:

- 1) We use a focal plane array (FPA) of 128 by 128 InSb (Indium Antimonide) detectors. FPAs combine state-of-the-art thermal and spatial resolution and are widely used for military applications. For applications such as non destructive testing 5,6, the cost of a FPA has often been prohibitive. In our case, however, all the equipment for the experiment was already available at our laboratory. Previously, using another FPA, the temperature profile of a blow fly was determined 7.
- 2) A second improvement described in this Paper, is the data analysis we use to compensate for variations in the emissivity of the semiconductor surface. Semiconductor surfaces typically have low and variable emissivities and can even be partly transparent. In the measurement described in this Paper, the surface incorporates both gold and (doped and non-doped) GaAs. For surfaces of about $100 \, ^{\circ}$ C, we are able to achieve an absolute temperature sensitivity of $\pm 5 \, ^{\circ}$ C, and determine small temperature differences of $1 \, ^{\circ}$ C.
- 3) Finally, we achieve good spatial resolution. In the raw data peaks are always at least 13 μ m wide due to the influence of the optics. Due to the high signal to noise ratio of our raw data we are able to deconvolute the data and attain a resolution of 6.25 μ m.

An alternative method of determining the temperature with micrometer resolution is by using liquid crystals ⁸. The device to be tested is coated with a thin layer of liquid crystals and then viewed through crossed polarisers and a microscope. The polarisation of the light reflected from the surface is determined by the temperature of the liquid crystal layer. Typically the device is first covered with a thin, black, uniform layer to compensate for differences in emissivity.

In principle, the use of liquid crystals in combination with an optical microscope offers superior spatial resolution. However, there are also major draw-backs: Firstly, the use of liquid crystals is rather awkward. Secondly, the applied layers on the device change the device's thermal and electrical properties under operating conditions. Finally, the influence of the applied layers remains even after the measurement, since the layers can not easily be removed.

2 THE GAAS MESFET

The device we chose to study was a gallium arsenide metal-semiconductor field-effect transistor (GaAs MESFET). The MESFET under test was manufactured using the Siemens DIOM process. We used a very large MESFET with 12 gate fingers and 1500 µm total gate width. This device is the major building component in the final stage of a high-power amplifier (HPA) monolithic microwave integrated circuit (MMIC). The MMIC operates at 10 GHz in the middle of the X-band. The monolithic integration allows such circuits to be cheaply and reproducibly manufactured for transmit-receive (TR) modules for phased-array radars.

The thermal design of a MESFET is very important for the device characteristics. The lifetime decreases very rapidly as the gate-finger temperature approaches 160 °C. With our measurement technique we can analyse its thermal behaviour.

For our measurements, the MESFET was soldered to a carrier (molybdenum/copper). The carrier was placed on top of a bronze chuck (gold-plated on top). The chuck was part of a commercial wafer prober (Alessi REL-4500). The wafer prober was used to connect the source, gate and drain voltages. A sketch of the set-up is shown in Fig. 1.

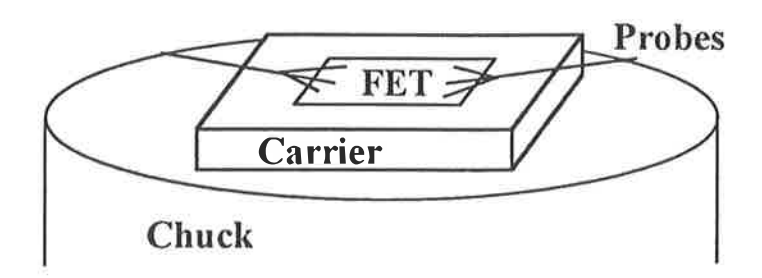


Figure 1: Sketch of the MESFET mounted on the carrier and chuck. Electrical connections are made with the probes. The chuck is thermally isolated and can be heated.

A top-view of the device under test is shown in the colour image of Fig. 2. This image was directly acquired with a charge-coupled device (CCD) camera: no image processing was performed. The light arrea is GaAs, the black and white parts are gold layers. The colour of the gold depends on how the gold layer has been processed. The gold-coloured (white) spots on the right and left of the image are due to scratches made while attaching the probes.

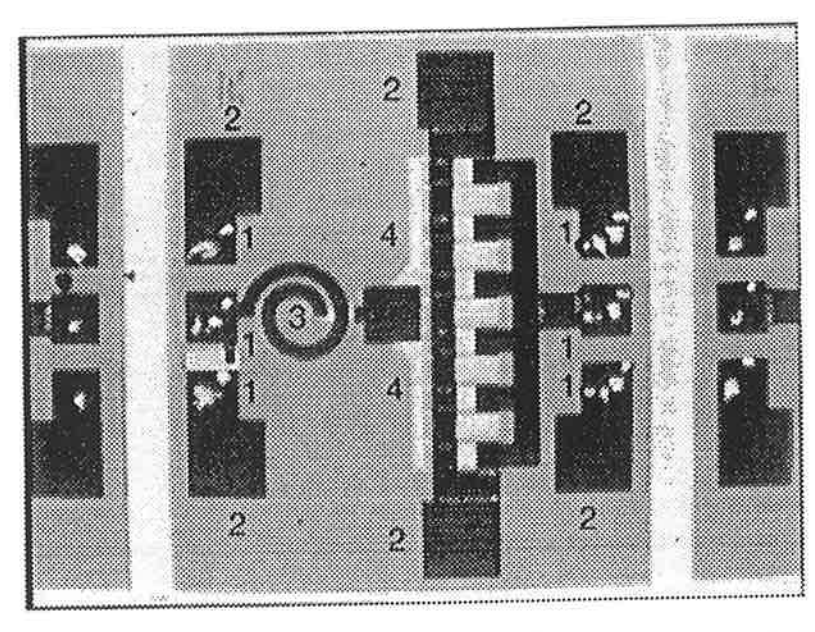


Figure 2: A top-view of the MESFET made with a CCD camera. Visible are: (1) probe pads, (2) via-holes, (3) spiral inductor, and (4) gate-fingers. The figure is flipped vertically with respect to Fig. 4 and Fig. 5.

Also visible are six square through-substrate via-holes (150 by 150 micron). The via-holes serve as DC and RF return path. In addition, the two via-holes connected to the MESFET serve as a thermal short. The spiral inductor visible on the left serves as a pre-matching structure and provides an acceptable return loss. As a result the RF source power could be limited to reasonable values. The inductor is, however, not relevant to the thermal behaviour of the MESFET itself.

The device is 100 µm thick with on top a thin layer doped GaAs. The material underneath is intrinsic GaAs. The interleaved gold structure consists of seven source areas, and six drain areas. In between each source and drain is a very narrow golden gate finger (0.8 µm gate length) inside a 9 µm band of n-doped GaAs. Each gate is separated 55 µm from the next. The entire device is covered with a thin, transparent layer of silicon nitride.

3 THE INFRARED CAMERA

For our measurements we used a commercial Amber 4128 Infrared camera system. The system incorporates a focal plane array (FPA) of 128 by 128 Indium Antimonide (InSb) detectors. The camera is sensitive to the photon flux in the 3 to 5 μ m wavelength band. The detectors are 50 μ m apart and have a similar spatial resolution.

A video signal allows live viewing of the images. For subsequent data analysis, the 12-bits digital data was averaged over 50 frames of data at 50 Hz and collected. This digital data was subsequently image processed and analysed.

A non-uniformity correction has been carried out on the pixels to compensate for variations in gain and offset of individual detectors. Some of these pixels are, however, 'uncorrectable'. They can be observed in the images since their response is very atypical.

4, OPTICAL SET-UP

Commercial infrared cameras are almost always combined with a lens that is designed for infinite conjugate ratio: an infinitely far-off object is imaged on the focal plane of the camera system: the angular resolution is important. In most cases where distant objects are imaged the angular resolution is most important. For the imaging of semiconductor devices, however, the absolute spatial resolution should be optimised.

Schematically, our optical set-up is shown in Fig. 3. A lens with a small focal length (f = 50 mm) was mounted just above the MESFET. The collimated beam was reflected by a mirror and subsequently focused by a second lens (f = 400 mm) onto the FPA. The difference in focal lengths of the two lenses causes the image on the FPA to be magnified by a factor of 8 onto the 50 μ m sized detectors. In this way the geometrically limited resolution is equal to 6.25 μ m.

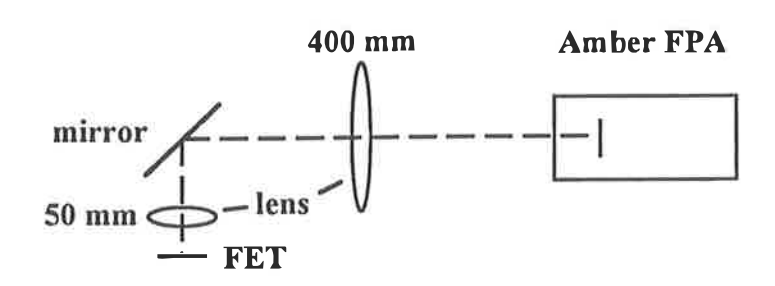


Figure 3: Optical set-up of the experiment. A magnified image of the MESFET is formed on the focal plane array (FPA).

However, in practice, for our infrared set-up, the resolution is hindered by diffraction of the optics. The Raleigh criterion for the diffraction limit states that the limiting resolution is equal to the product of the wavelength of the light λ , a constant of the order of one and the f-number (= f/d) of the optical system.

$$\Delta x = 1.22 \times \lambda \times f/d \tag{1}$$

Therefore the speed of the first lens is most critical. In practice, we used a lens with an f-number of 2.3, so that the diffraction-limited resolution for our set-up is about $13 \mu m$.

5 CALIBRATION PHILOSOPHY

Unfortunately, the measurement technique does not allow us to measure the temperature directly. Rather we measure the infrared flux emitted and reflected by the device. The detected flux depends on the emissivity of the surface and non linearly on the temperature of the emitting surface. Fortunately, the non linearity of the emitted flux as a function of temperature can be calculated. Our solution to the variation of emissivity and reflectance over the surface is to incorporate this variation in our calibration.

Previously, we performed a similar study ⁹ to determine the temperature of a diode micro structure. In that case, the surface of interest was molybdenum and a similar large sample of this material was available. Its emissivity was measured to be 10%, in accordance with values quoted in the literature. Once the emissivity is known, the so called apparent temperature (the temperature measured relative to that of a 100% emitting surface), could be converted to an actual temperature.

For the present experiment such a calibration would be difficult since the emissivities of the gold structures (about 3%) are much smaller than the 10% of molybdenum 10, and hence a small uncertainty in the reflectivity (reflectivity = 1 - emissivity) would lead to a large uncertainty in the actual device temperature.

Our solution to the variation of emissivity over the surface was to take calibration images at constant known temperatures. This was possible since the thermally-isolated chuck of the wafer prober allows the entire device to be heated to a uniform temperature. A possible error introduced by this technique is that the MESFET moves when the chuck or carrier expands during heating. Indeed, we were obliged to compensate for such an effect.

6 FLUX NON LINEARITY

From the acquired data we want to derive the temperature. The measured signal, however, is linear in the number of incident photons. To find the non linear increase of photon flux with temperature, we calculated the photon flux in the wavelength band for which our camera is sensitive (3 to 5 μ m). The integrated result for the photon flux, was fitted to an analytic curve of the following shape:

$$\Phi = C_1 + C_2 \times T^{\mathsf{n}} \tag{2}$$

The constants C_1 and C_2 are fitted to the fluxes at 60 °C and 100 °C. A value for n of 8.5 gives almost perfect agreement. It is well known that the *total* photon flux increases as T^3 . The additional increase in this case occurs because the maximum of the Planck curve shifts towards the 3 to 5 μ m band.

7 RAW DATA

Initially, our experiments focused on observing the heating effect of turning on DC voltages at ambient temperatures. This should lead to additional local heating near the gate fingers. Fig. 4 shows the GaAs MESFET, at ambient temperature (25 °C), at similar magnification as the optical image of Fig. 2 but now imaged with our infrared set-up. The bar at the top shows how dark correspond to small flux and the brighter correspond to high flux. The square box (200 μ m by 200 μ m) in the lower left quarter of the image denotes the scale of the image.

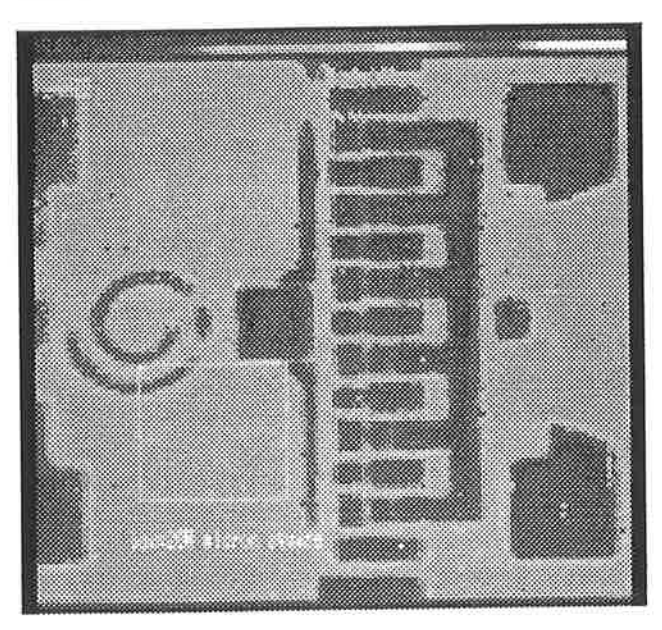


Figure 4: Infrared image of the GaAs MESFET at ambient temperature (25 °C). Dark corresponds to little flux and light corresponds to more flux. The square box denotes the scale of the image.

Turning on the DC voltages, results in the image of Fig. 5. Indeed the lighter parts of the image correspond to areas of GaAs near the narrow gates from where an increased amount of flux is emitted. In addition, the gold source and drain structures are also increased in temperature: their colour has changed slightly.

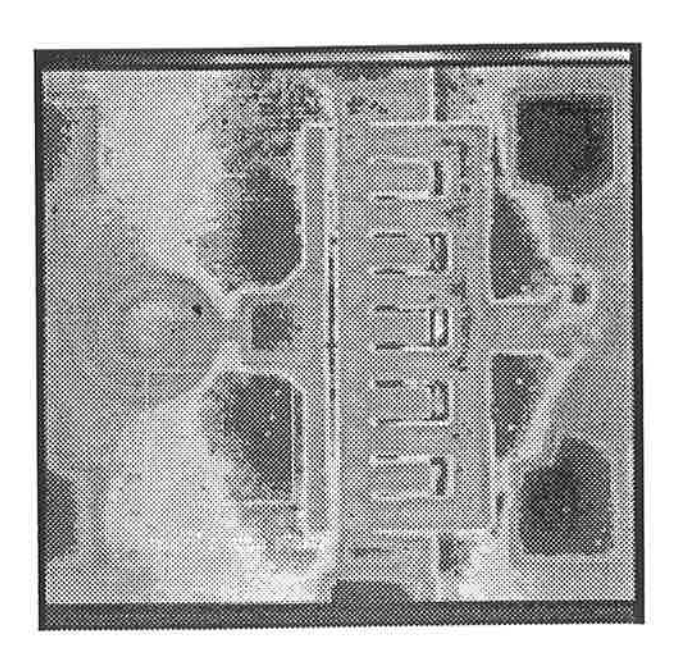


Figure 5: Infrared image of the MESFET with DC voltages turned on. The lighter parts of the image correspond to the hotter areas of GaAs near the narrow gate fingers.

Under operating conditions the carrier, and therefore the base plate of the device, is held at a constant 60 °C in temperature. For the determination of the MESFET temperature under normal operating conditions a digital set of data was acquired:

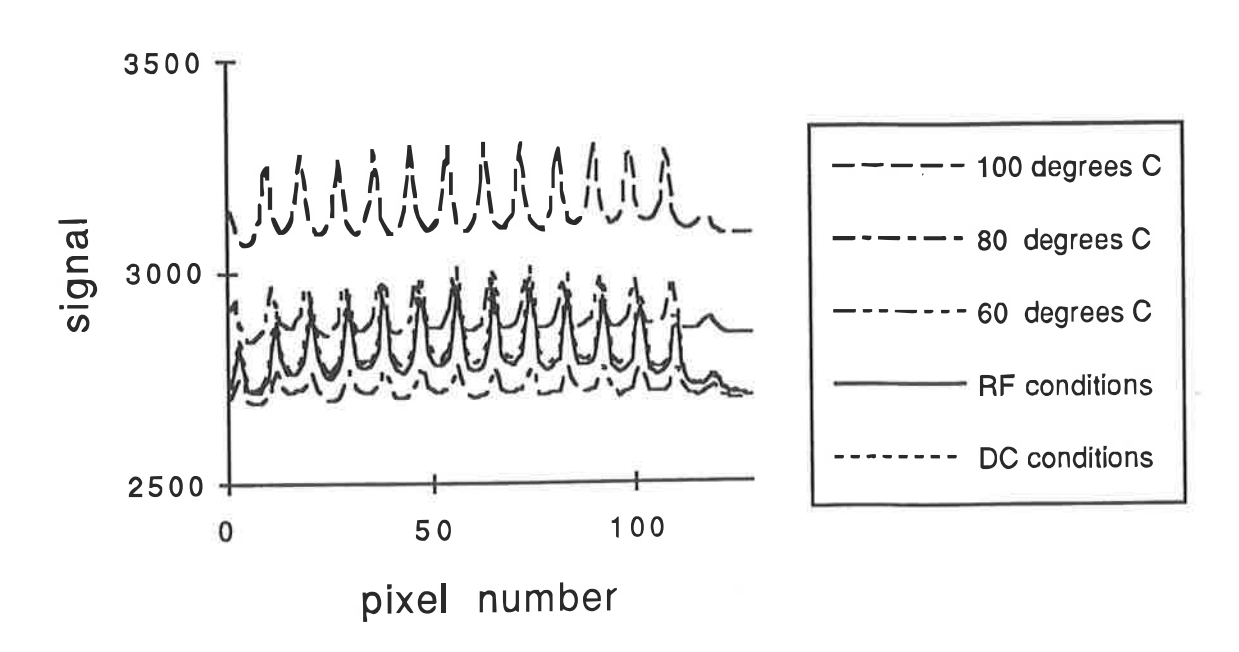


Figure 6: 12-bits raw data for five different conditions. The 12 gates can easily be discerned. The modulation over the line for the data at constant temperature reflects the change in emissivity of the surface. The more pronounced modulation for the RF and DC conditions reflects the local extra heating near the gate fingers. Low pixel numbers correspond to the top of Fig. 4 and Fig. 5.

For the first measurement, DC bias voltages were applied (class A bias point), while the base plate was kept at 60 °C. For the second measurement, RF power was applied in addition to the DC bias voltages, while again the base plate was held at 60 °C. Finally, three calibration measurements were performed with the MESFET heated to 60 °C, 80 °C and 100 °C, without any DC voltages or RF power.

For an accurate determination of the MESFET temperature we selected the thermally interesting line of pixels through the middle of the interleaved structure. The raw 12-bits data for the five different conditions are shown in Fig. 6. We indeed see that the signal increases non linearly as the temperature is increased from 60 °C to 100 °C. The modulation over the line for the data at constant temperature reflects the change in emissivity of the surface. For the RF and DC conditions, the modulation is even more pronounced. This additional modulation reflects the local extra heating near the gate fingers. The 12 gates can easily be discerned.

Another observable effect is that the peaks in the modulated structure seem to shift to lower pixel numbers for higher temperatures. This displacement is caused by thermal expansion. Under DC and RF conditions this displacement does not occur since the chuck temperature is kept at 60 °C. In actual fact, for the 100 °C condition there is an overall displacement of two pixels to the left and two pixels to the top. For the subsequent analysis we compensated for the thermal expansion by translating the measured images.

8 SPATIAL RESOLUTION AND DECONVOLUTION

The spatial resolution of our measured raw data is not infinitely small. The peaks have a width of about 13 μ m (FWHM) due to optical diffraction. However, we were able to deconvolute the influence of the lens.

The fourier transform of the data was divided by the MTF of the lens. The MTF was not measured directly but rather we assumed the MTF of a diffraction-limited lens. For our purposes this assumption is justified. Subsequently, the data was fourier transformed back again.

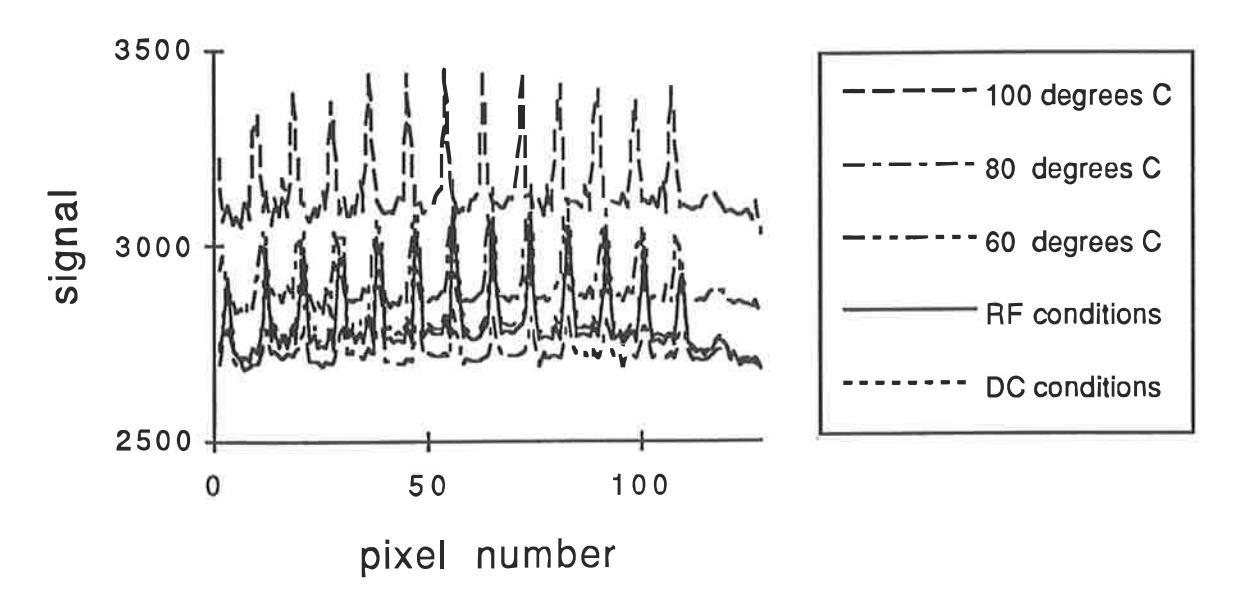


Figure 7: The raw data after deconvolution. By compensating for diffraction of the optical set-up, the spatial resolution can be improved from $13 \mu m$ to $6.25 \mu m$.

In this way we attain a spatial resolution of about 6.25 μ m. This is better than the commonly stated diffraction limit, according to the Raleigh criterion (13 μ m). However, the frequency that corresponds to 6.25 μ m is still below the frequency cutoff of our lens.

The raw data after deconvolution is shown in Fig. 7. The peaks are now appreciably narrower, although the data seems noisier. Unfortunately, the obtained spatial resolution is still much larger than the width of the gate fingers (0.8 µm). Therefore, we do not determine the temperature of the gate finger itself, but rather some spatial average over its surroundings.

<u>9 COMPENSATION FOR TRANSPARENCY OF GAAS</u>

A problem, whose full extent only became apparent after the measurements, is that the most interesting and highest temperatures are encountered on the n-doped GaAs surfaces. Unfortunately this surface is highly transparent. According to the literature 11 the intrinsic GaAs layer is completely transparent. The GaAs layer on top near the gate fingers, however, is heavily doped and mixed with various impurities, and will be partly emitting (typically about 1%) 12.

A temperature for the n-doped GaAs can be assigned if we assume that the measured flux is the sum of the emitting GaAs and the emitted flux from the gold back layer of the device. In addition, we assume that under operating conditions the back surface remains at 60° C.

$$\Phi(T) = (1 - \%GaAs) \times \{C_{1,gold} + C_{2,gold} \times (273.15 + T)^{8.5}\}$$

$$+ \%GaAs \times \{C_{1,GaAs} + C_{2,GaAs} \times (273.15 + T)^{8.5}\}$$

$$+ \%GaAs \times \{C_{1,gold} + C_{2,gold} \times (273.15 + 60)^{8.5}\}$$
(3)

For the extracted line we can determine a maximum ($\Delta\Phi_{max}$) and minimum difference ($\Delta\Phi_{min}$) in flux between the 60 °C and 100 °C measurements. The maximum difference corresponds with 100% GaAs and the minimum with 0% GaAs. For every individual pixel on the line, the difference in flux ($\Delta\Phi_i$) corresponds to the percentage GaAs:

$$\%GaAs = \frac{\Delta\Phi_{i} - \Delta\Phi_{min}}{\Delta\Phi_{max} - \Delta\Phi_{min}}$$
 (4)

From our data we find that the maximum change in flux is 1.93 times as large as the minimum change. Since the emissivity of gold is about 3%, the emissivity of n-doped GaAs plus the gold back layer is about 5.8 % and the emissivity of the GaAs by itself is 2.8 %.

From the pixel with minimum flux difference we can extract the constants C_1 and C_2 for gold:

$$C_{1,\text{gold}} = \frac{\Phi(60) \times (273.15 + 100)^{8.5} - \Phi(100) \times (273 + 60)^{8.5}}{(273.15 + 100)^{8.5} - (273 + 60)^{8.5}}$$
(5)

$$C_{2,\text{gold}} = \frac{\Phi(100) - \Phi(60)}{(273.15 + 100)^{8.5} - (273 + 60)^{8.5}}$$
(6)

From the pixel with maximum flux difference we find $C_{1,GaAs} + C_{1,gold}$, and $C_{2,GaAs} + C_{2,gold}$, using formulas (5) and (6).

Once these constants are known we can determine the temperature for every pixel. The calibrated thermal profile, calculated in this way, for the line through the gate fingers is shown in Fig. 8.

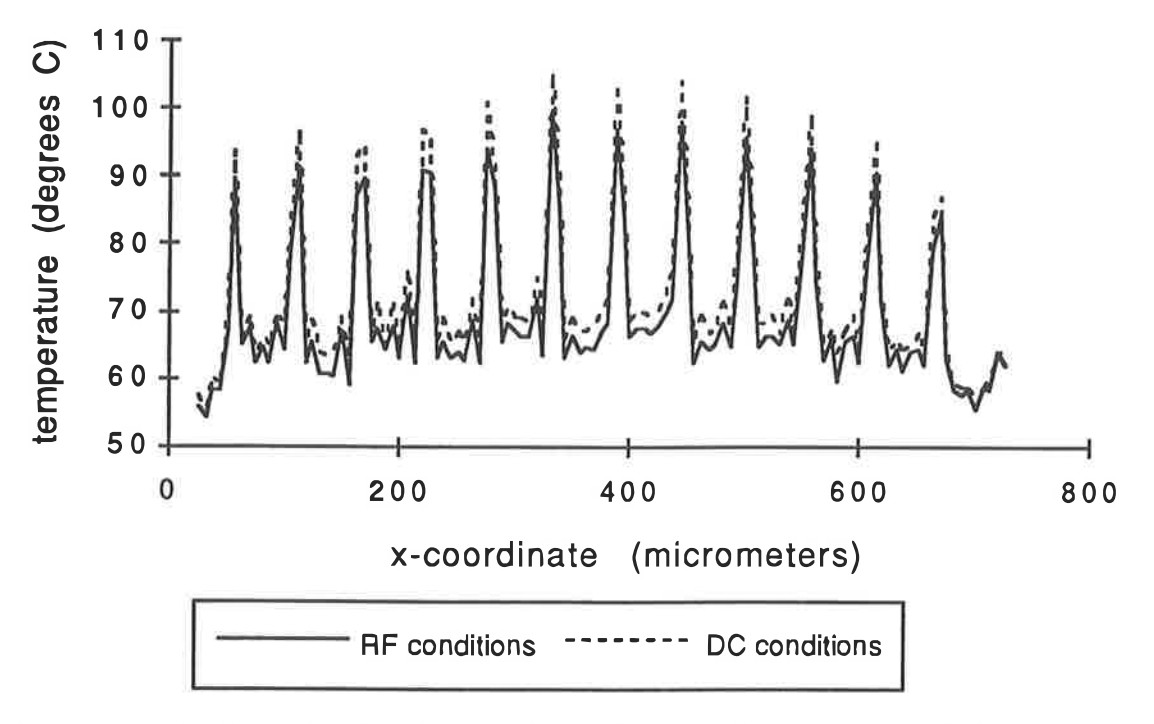


Figure 8: The thermal profile for the line through the gate fingers for a base-plate temperature of 60 °C. The data is compensated for the variation of emissivity between the opaque, highly reflecting gold surface and the transparent GaAs surface. A small x-coordinate corresponds to the top of Fig. 4 and Fig. 5. The change in temperature from DC to RF conditions reflects the decrease in dissipated power.

10 DISCUSSION

In Fig. 8, we see that the temperature in the middle of the interleaved structure is higher than at the edges. The higher temperature in the middle is expected since the distance to the nearest via-hole, that partly serves as a heat sink, is further. However, the difference is only small since the gate to gate spacing of 55 μ m is relatively large. A much larger effect would be expected if the spacing were smaller than 20 μ m 3 .

In Fig. 8, we also observe that turning on the RF power leads to cooling of the MESFET. The measured temperature is largely determined by the power dissipated by the MESFET, and the thermal resistance between the MESFET on the top of the device and the gold base of the device. Thermal radiation is not a dominant contribution to the heat flow.

We will now calculate the power dissipated in the MESFET under DC and RF conditions. For the DC case, a drain voltage of 6 V was used. In combination with a current of 228 mA this resulted in a dissipated power of 1.37 W.

Under RF conditions, the RF power going into the device (RF_{in}) was 161 mW and the RF power delivered to load (RF_{out}) was 308 mW. As a result of the RF power, the DC current decreased slightly to 225 mA while the DC voltage remained at 6 V (DC_{in} = 1.35 W). Therefore, under RF conditions, the dissipated power is decreased to 1.20 W. This decrease in dissipated power is largely caused by DC power being converted into amplified RF power that is not dissipated inside the MESFET

In accordance with our measurements, this calculation shows that turning on the RF power leads to cooling. Although the power added efficiency was only 11% (PAE = $(RF_{out} - RF_{in}) / DC_{in}$), the cooling can nevertheless be clearly observed.

If we assume that the thermal resistance is approximately constant as a function of temperature, then the decrease in dissipated power of 12%, should lead to a similar change of temperature with respect to the base-plate temperature of 60 °C. Indeed, in Fig. 8 we observe a similarly sized decrease ($14\% \pm 3\%$).

11 ERROR ANALYSIS

Several sources of errors combine in the results of Fig. 8. Since the emissitivity of the MESFET is so low we were first afraid that the photon noise might be a dominant error source. However, the low emissivity is partly compensated by the high temperatures we are measuring at. By averaging over 50 frames we make sure that the photon noise is not a dominant error source.

The thermal resolution corresponding to one bit is also not a dominant error source. From Fig. 6 we see that, for a gold area with 3% emissivity, a temperature difference of 20 degrees corresponds to about 300 bits, i.e. 1 bit corresponds to 67 mK. For the n-doped GaAs near the gate fingers, the emissivity has a similar value and therefore the contribution due to the digitisation can be neglected.

A source of error could also be variations in the background temperature since we are for more than 90% sensitive to the ambient surroundings. The influence of laboratory heat sources was minimised by shielding the set-up. In addition, the data was acquired as rapidly as possible so that no large changes in the ambient temperature could occur.

The compensation for the non uniformity works fairly well. As a test we checked to see how well the interpolation of the data at 80 °C worked. The result was 80 ± 5 °C and incorporates all the above mentioned error sources. Therefore we conclude that our results are also determined to an absolute accuracy of \pm 5 °C.

This error in the absolute temperature is largely dominated by the thermal expansion of the chuck during the calibration measurements. In addition, it will depend on the device temperature and the emissivity. The relative temperature difference between DC and RF conditions is independent of the thermal expansion and will be more accurate.

This relative error can be deduced from the relative change in temperature difference between gate fingers and the base plate by changing from DC to RF conditions. If we assume this relative decrease to be the same for the 12 gate fingers then the measured decrease of $14\% \pm 3\%$ corresponds to a relative accuracy of ± 1 °C.

12 CONCLUSIONS

In conclusion, we are able to non invasively determine absolute temperatures of semiconductor devices by using a FPA. The spatial resolution (6.25 μ m) is shown to be sufficient for the imaging of individual gate fingers for actual devices. We have also shown how to reliably determine the temperature of opaque and transparent surfaces with varying low emissivities.

Acknowledgements

The authors wish to thank Dr. E. Pettenpaul and T. Meier from Siemens Semiconductors in München for supplying the MESFET devices. In addition we would like to thank Rob Kemp for providing the digital data-acquisition software.

REFERENCES

- [1] S.H. Wemple and H. Huang, "Thermal Design of Power GaAs FETs", Chap. 5 in GaAs FET Principles and Technology, J.V. DiLorenzo and D.D. Khandelwal, Eds., pp. 309-348, Artech House, Dedham, MA (1982).
- [2] G. Clerico Titinet and P.M. Scalafiotti, "Temperature Distribution on GaAs MESFETs: Thermal Modeling and Experimental Results", in *Semiconductor Device Reliability*, A. Christou and B.A. Unger, Eds., pp. 479-489, Kluwer, Amsterdam, The Netherlands (1990).
- [3] H.F. Cooke, "Thermal Effects and Reliability" (photo courtesy of Y. Aoki), Chap. 5 in High-Power GaAs FET Amplifiers, J.L.B. Walker, Ed., pp. 227-261, Artech House, Norwood, MA (1993).
- [4] J. Caniou, L'observation et le mesurage par thermographie, pp. 218-219, AFNOR, Paris, France (1991).
- [5] L. West, "Infrared Nondestructive Testing: A New Aid for Manufacturing", Photonics Spectra 28 (10), 101-106 (1994).
- [6] M.K. Lang, G.W. Donohoe, S. H. Zaidi, S.R.J. Brueck, "Real-time image processing techniques for noncontact temperature measurement", Optical Engineering 33 (10), 3465-3470 (1994).
- [7] D.G. Stavenga, P.B.W. Schwering, and J. Tinbergen, "A Three-Compartment Model Describing Temperature Changes in Tethered Flying Blowflies", *Journal of Experimental Biology* 185, 325-333 (1993).
- [8] J. Rodriguez Tellez, S. Loredo, and R.W. Clarke, "Self-Heating in GaAs FETs: A Problem?", Microwave Journal 37 (9), 76-92 (1994).
- [9] M.P. de Boer, H. Winkel, and J.S. de Vries, "Apparent and Actual Temperature Determination of Molybdenum Diode Micro Structures", (unpublished), (1994).
- [10] American Institute of Physics Handbook, 2nd edition, McGraw-Hill, New York, NY (1957).
- [11] D.R. Wight, "The physical and electronic properties of GaAs", Chap. 1 in *Gallium Arsenide*, M.J. Howes and D.V. Morgan, Eds., pp. 1-38, Wiley, Chichester, UK (1985).
- [12] H. Y. Fan, "Effects of Free carriers on the Optical Properties", Chap. 9 in Semiconductors and Semimetals Volume 3 (Optical Properties of III-V Compounds), R.K. Willardson and A.C. Beer, Eds., pp. 406-420, Academic Press, New York, NY (1967).